Chapter 3. Millimeter-wave, Terahertz, and Infrared Devices

Academic and Research Staff

Professor Qing Hu

Visiting Scientists and Research Affiliates

Dr. Gerhard de Lange

Graduate Students

Erik K. Duerr, Konstantinos Konistis, Ilya Lyubomirsky, Brian P. Riely, Benjamin S. Williams, Bin Xu, Noah D. Zamdmer

3.1 Introduction

Millimeter-wave and THz frequencies (f > 100 GHz) remain one of the most underdeveloped frequency ranges, even though potential applications in remote sensing, spectroscopy, plasma diagnostics, and communications are obviously great. This is because the millimeter wave and far-infrared frequency range falls between two other frequency ranges in which conventional semiconductor devices are usually operated. One is the microwave frequency range, and the other is the near-infrared and optical frequency range. Semiconductor devices which utilize the classical diffusive transport of electrons, such as diodes and transistors, have a high frequency limit. This limit is set by the transient time and parasitic RC time constants. Currently, electron mobility and the smallest feature size which can be fabricated by lithography limit the frequency range to below several hundred GHz. Semiconductor devices based on quantum mechanical interband transitions, however, are limited to frequencies higher than those corresponding to the semiconductor energy gap, which is higher than 10 THz for most bulk semiconductors. Therefore, a large gap exists from 100 GHz to 10 THz in which very few devices are available.

Semiconductor quantum-effect devices, which can be loosely termed “artificial atoms,” including both vertically grown quantum-well structures and laterally confined mesoscopic devices, are human-made quantum mechanical systems in which the energy levels can be chosen by changing the sizes of the devices. Typically, the frequency corresponding to the intersubband transitions is in the millimeter-wave range (ΔE ~ 1-4 meV) for the lateral quantum-effective devices, and the THz to infrared range for the vertical quantum wells. It is therefore appealing to develop ultrahigh-frequency devices, such as radiation detectors and mixers, and THz and infrared lasers utilizing the intersubband transitions in these devices.

In addition to new physical concepts, novel technologies must also be developed to meet the challenges at these high frequencies. Conventional mechanically machined horn antennas integrated with waveguide cavities have been the workhorse at microwave and millimeter-wave frequencies since they were first implemented more than fifty years ago during World War II. Very high antenna gain and essentially perfect antenna efficiency can be achieved using these structures. However, they are expensive, bulky, and incompatible with arrays. In order to overcome these problems, new development has been made to use micromachining to fabricate the horn antenna structures.

In these structures, the active elements and their planar antennas are fabricated on a free-standing thin (~1 micron) SiN membrane, which is suspended over a silicon pyramidal horn that is formed by anisotropic etching, or micromachining. The side walls of this micromachined structure can then be coated with Au to form a horn antenna. Compared to conventional waveguide horn antennas, this novel micromachined structure has several major advantages. It is easier to fabricate fine three-dimensional structures by using photolithography. Horn antennas with micron precision can be easily defined and inexpensively mass produced. They are made on Si or GaAs wafers and compatible with thin-film technology. Thus, active elements, such as RF and IF amplifiers, mixers and video detectors, local oscillators, and post-detection signal processors, can be integrated monolithically with the antenna structures to form monolithic transmitter/receiver systems. The micromachined antenna is lightweight and compact. The most attractive feature of the micromachined struc-

ture is that focal-plane arrays can be fabricated easily on a single wafer, as illustrated in Figure 1b. Such systems will yield a significantly improved spatial resolution in remote sensing and a much greater antenna gain when implemented with phased-arrays.

Our group is systematically investigating physical and engineering issues that are relevant to devices operating from millimeter-wave to infrared frequencies. Specifically, we are working on micromachined millimeter-wave focal-plane arrays and development of terahertz and infrared lasers based on intersubband transitions.

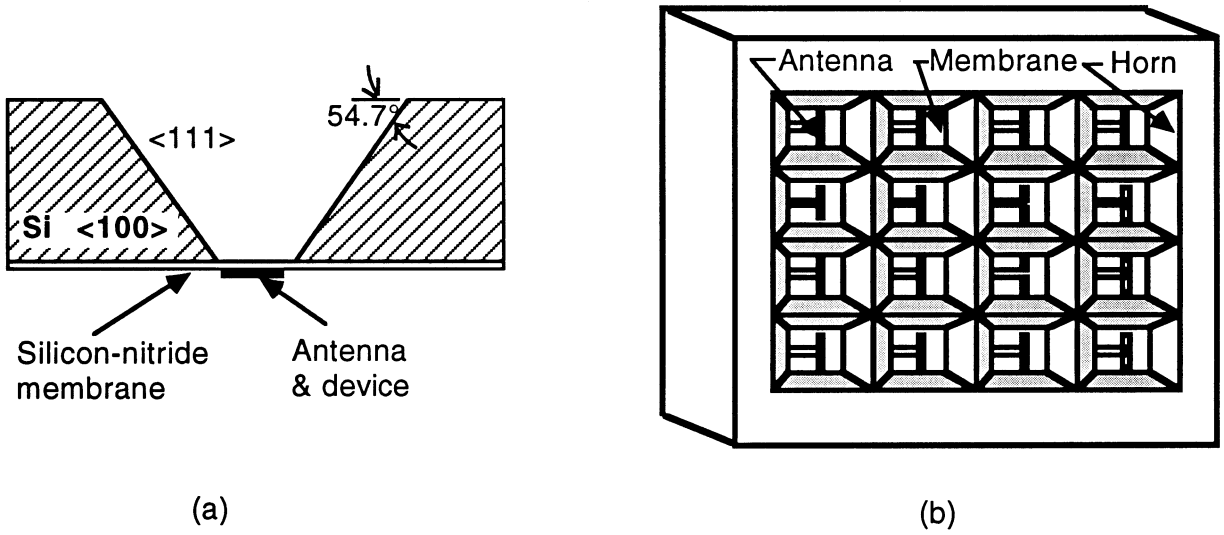

Figure 1. (a) Example of a micromachined horn antenna structure that is made by anisotropically etching a <100> silicon wafer. (b) Schematic of a focal-plane array on a single wafer made using micromachining.

3.2 Micromachined SIS millimeter-wave Focal-plane arrays

Sponsors

National Science Foundation
Grant AST 94-23608
National Aeronautics and Space Administration
Grant NAGW-4691

Project Staff

Dr. Gerhard de Lange, Kostantinos Konistis, Professor Qing Hu, in collaboration with Dr. Gerry Sollner and Group 86,[1] Dr. Ray Robertazzi,[2] Dr. David Osterman[2]

Superconductor-insulator-superconductor (SIS) heterodyne receivers have been demonstrated to be the most sensitive receivers throughout the 30-840 GHz frequency range. The challenge now in the SIS receiver technology is to develop focal-plane arrays to improve the efficiency of data acquisition. In order to achieve these goals, we are currently developing a novel scheme to couple the millimeter-wave and infrared signals to the superconducting devices by using a micromachined horn antenna and a planar antenna supported by a thin (~1 micron) membrane, as shown in Figure 1a. As stated in the introduction, this novel micromachined antenna structure can be produced with a high precision using photolithography, and it can be utilized in focal-plane arrays, as shown in Figure 1b.

Following our recent success in developing single-element micromachined SIS receivers,[3] we have designed and constructed a 3x3 focal-plane array with the center frequency around 200 GHz. The schematic of the structure is shown in Figure 2, which includes a micromachined and mechanically

1 MIT Lincoln Laboratory, Lexington, Massachusetts.

2 HYPRES, Inc., Elmsford, New York.

3 G. de Lange, B.R. Jacobson, and Q. Hu, "A Low-noise Micromachined Millimeter-wave Heterodyne Mixer with Nb Superconducting Tunnel Junctions," *Appl. Phys. Lett.* 68: 1862 (1996).

machined horn array, the device wafer, and the dc and IF connection board. Measurements of the dc I-V characteristics showed good uniformity across the entire array. A heterodyne measurement on the central element yielded the best result. The minimum uncorrected receiver noise temperature is 52 K DSB, measured at a bath temperature of 2.7 K. This noise temperature is comparable to the best results obtained in (tunable) waveguide mixers.

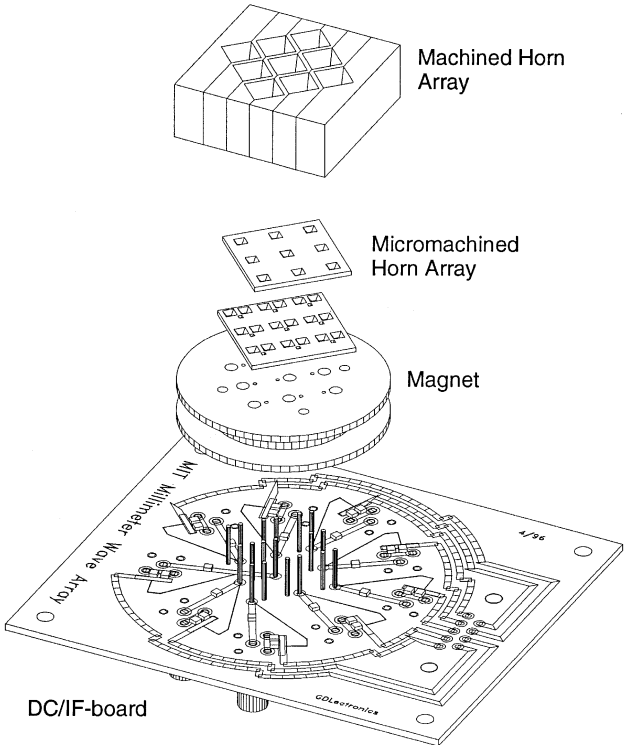

Figure 2. (a) Schematic of an array structure including a micromachined and machined horn array, the device wafer, and the dc and IF connection board. (b) I-V curves of seven SIS junctions in the array.

The measured noise temperatures as functions of the LO frequency for all nine elements of another array are shown in Figure 3. In this array the minimum noise temperature of the central element is 62 K (illustrated in the inset). The measured noise temperature of the different elements is fairly uniform, with minimum noise temperatures for all the nine elements ranging from 62 to 101 K. The 3-dB noise bandwidth of all nine elements has a uniform value of 30 GHz across the array. We attribute the slight difference in the noise temperatures to the effect of the limited size of our dewar window and the thick lens inside the dewar. Measurements of several arrays always showed the lowest noise temperature for the central element.

The DSB noise temperatures of the current state-of-the-art waveguide receivers for the 230 GHz astronomy band are in the range of 35-50 K. With a further optimization of the junction device characteristics and a reduction of the junction area, the micromachined SIS mixer arrays could yield comparable noise temperature for each array element. Furthermore, the scalability of the machined and micromachined sections could extend the operating frequencies of the micromachined focal-plane imaging arrays up to 1 THz.

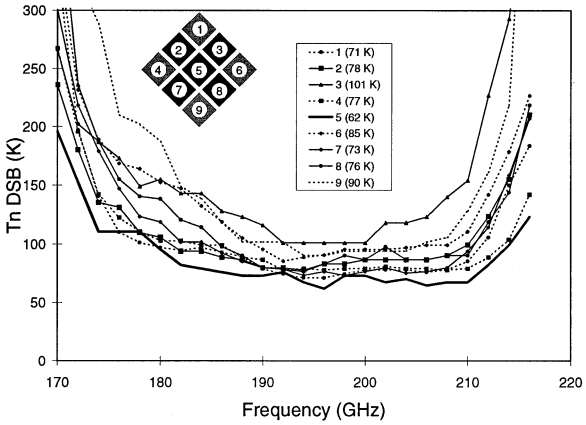

Figure 3. Measured DSB noise temperatures of all the nine elements in the array. The inset shows the minimum noise temperature for each element.

3.3 Intersubband-transitions Lasers

3.3.1 Electrically Pumped THz Emitters using Quantum Wells

Sponsor

U.S. Army Research Office
Grant DAAH04-95-1-0610

Project Staff

Bin Xu, Benjamin S. Williams, Professor Qing Hu, in collaboration with Professor Michael R. Melloch[4]

Semiconductor quantum wells are human-made quantum mechanical systems in which the energy levels can be designed and engineered to be of any

4 Purdue University, West Lafayette, Indiana.

value. Consequently, unipolar lasers based on intersubband transitions (electrons that make lasing transitions between subband levels within the conduction band) were proposed for long-wavelength sources as early as the 1970s. However, because of the great challenge in epitaxial material growth and the unfavorable fast nonradiative relaxation rate, unipolar intersubband-transition lasers (also called quantum-cascade lasers) at near-infrared (4-5 micron) and mid-infrared (8-11 micron) wavelengths were developed only recently at Bell Laboratories.

This achievement is remarkable, but the technique used in the original quantum-cascade lasers will not be directly applicable for the longer-wavelength THz range because of two major obstacles. First, the energy levels corresponding to THz frequencies (1 THz = 4 meV) are quite narrow, so the requirements for the design and fabrication of suitable quantum wells are demanding. Because of the narrow separation between subband levels, heating and hot-electron tunneling will have a much greater effect. Also, the small energy scales of THz photons make the detection and analysis of spontaneous emission (a crucial step toward developing lasers) quite difficult. Second, and perhaps most important, mode confinement, which is essential for any laser oscillation, is difficult at longer wavelengths. Conventional dielectric-waveguide confinement is not applicable because the evanescent field penetration, proportional to the wavelength and on the order of several tens of microns, is much greater than the active gain medium of several microns. We are currently developing intersubband-transition lasers based on our recent success in generating and detecting THz emission signals and a novel mode confinement method using metallic waveguide structures.

Our MQW structure for THz emission is shown in Figure 4, in which the conduction band profile and the square of the wave functions were calculated self-consistently from Schrödinger and Poisson equations. The device is formed by a triple-well structure using GaAs/$Al_{0.3}Ga_{0.7}As$ materials, as shown in the dashed box. This structure is essentially a three-level system, which is required for any laser. These are marked as E_3, E_2, and E_1 in Figure 4; the level E_4 is much higher in energy so it does not contribute to transport at low biases. Because there is no recombination involved in unipolar intersubband lasers, electrons can be "reused" many times. Consequently, many identical triple-well modules can be cascade-connected, and the emission power and the mode confinement factor can be increased substantially. Due to translational symmetry, design analysis needs to focus only on one module, provided there are no global space charges and high-field domains.

The collector barrier (which has a 2.0-nm thickness) is center δ-doped at approximately $10^{11}/cm^2$ in order to provide dynamic charges to assure a global charge neutrality. The radiative transition takes place between E_3 and E_2, with an energy separation of $\Delta E_{32} \approx$ 14 meV and an oscillator strength of $f_{32} \approx$ 0.31 using the effective mass in GaAs. Under the designed bias of 50 mV per module, the ground state E_1' of a previous module is aligned with E_3. Thus, the upper subband E_3 can be selectively populated through resonant tunneling. The energy separation between E_2 and E_1 was designed to be 36 meV under the bias, which corresponds to the LO-phonon energy $\hbar\omega_{LO}$ in GaAs. Once energetically allowed, the very fast LO-phonon scattering with a time $\tau_{21} \approx$ 1.4 ps will rapidly depopulate the E_2 level and establish a population inversion between E_3 and E_2.

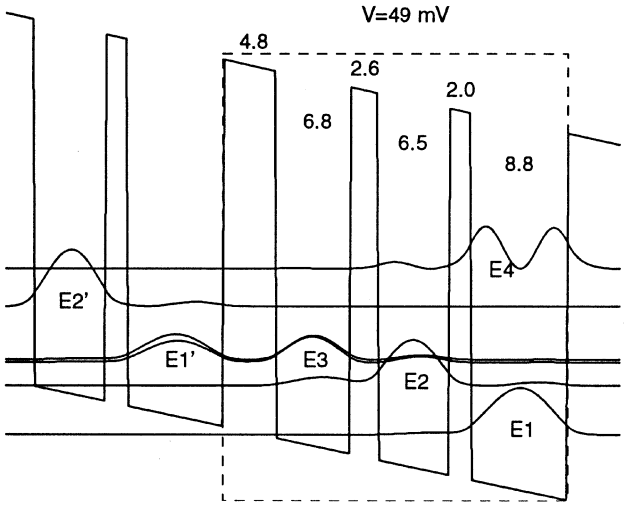

Figure 4. Schematic of a three-level system based on a triple quantum-well structure. The radiation transition takes place between E_3 and E_2, and the fast LO-phonon emission keeps the level E_2 empty. The conduction-band profile and the square of the electron wavefunctions were calculated numerically from Schrödinger and Poisson equations.

The MQW structures were grown in the molecular-beam-epitaxy (MBE) machine by our collaborator Professor Michael R. Melloch and his group at Purdue University. In order to verify the accuracy of our design calculations and to inspect the quality of quantum wells and interfaces, we performed an infrared absorption measurement with the result shown in Figure 5. The measurement was performed on a 80-module device (with a total of 240 quantum wells) at

room temperature. A mid-infrared absorption peak is clearly seen at 110 meV, which is due to the intersubband transition from E_1 to E_4. The FWHM is only 7 meV, including a 4-meV instrumental linewidth. This narrow linewidth is an indication of the high quality and uniformity of the wells and interfaces. Furthermore, the measured $E_1 \rightarrow E_4$ transition frequency of 110 meV and the dipole moment of 14 Å (deduced from the area of the absorption peak) agreed quite well with the calculated values of 109 meV and 12 Å, indicating the accuracy of our calculations.

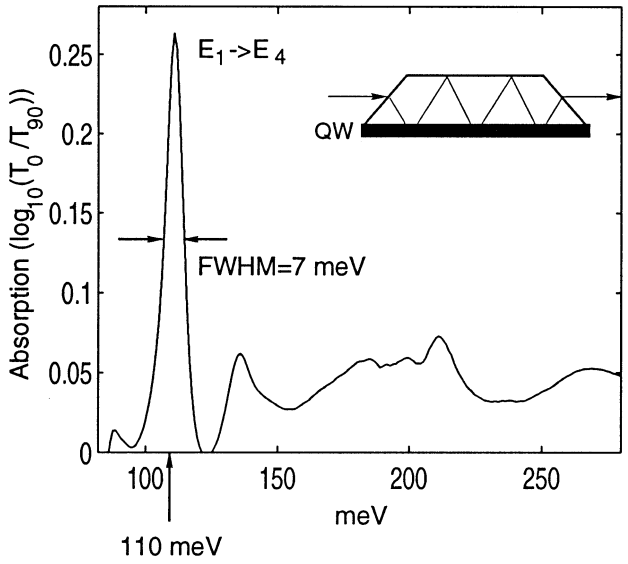

Figure 5. Infrared absorption measurement of a 80-module device, which was placed at room temperature. The absorption peak is due to the $E_1 \rightarrow E_4$ intersubband transition. The measured FWHM is 7 meV, including a 4-meV instrumental linewidth. The measured intersubband transition frequency (110 meV) and dipole moment (14 Å) agreed quite well with the calculated values of 109 meV and 12 Å.

In order to measure the intersubband THz emission and resolve its spectra, we constructed a set up that included an external Fourier transform infrared spectrometer (FTIR) with a composite Si bolometer as its detector. The system schematic is shown in Figure 6. We have improved this system and perfected our measurement techniques so that THz emission measurements can be routinely performed on our emitters with output power levels of 1-10 pW.

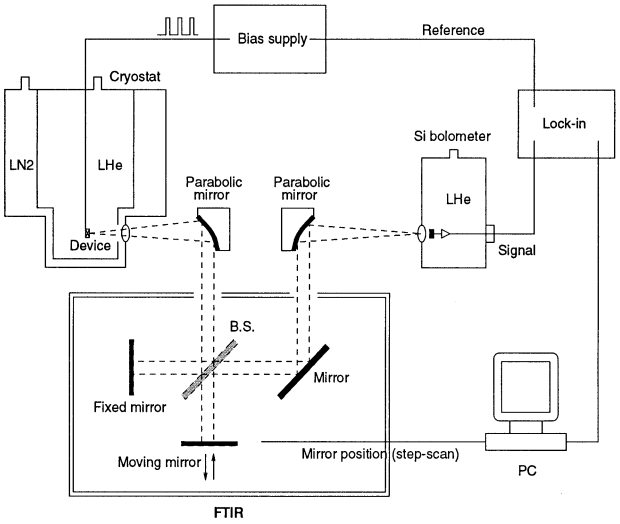

Figure 6. Far-infrared measurement set-up that uses an external Fourier transform spectrometer to spectrally resolve the emitted THz signals.

3.3.2 Optically Pumped THz Emitters using Quantum Wells

Sponsors

U.S. Army Research Office/AASERT
Grant DAAH04-94-G-0167
Hertz Foundation Fellowship

Project Staff

Ilya Lyubomirsky, Professor Qing Hu, in collaboration with Professor Michael R. Melloch[5]

Compared to electrical pumping, optical pumping offers advantages of easier design, higher selectivity in pumping, and separation of the pump and electrical bias. For THz emitters, easily available CO_2 lasers can be used as the pumping source. We first designed a three-level system for THz emission. However, this structure showed excessive heating when pumped by an intense CO_2 laser. In order to increase the emission efficiency and therefore the gain of the active medium, we have redesigned our optically pumped THz emitters based on a four-level system using coupled triple quantum wells, as shown in Figure 7. Electrons on the ground state E_1 can be pumped by a CO_2 laser to the E_4 level. By carefully engineering the scattering rates between subband levels by choosing subband energy separations and spatial locations, a population inversion between E_3

5 Purdue University, West Lafayette, Indiana.

and E_2 can be achieved. It was estimated that a modal gain of approximately 100 cm^{-1} can be achieved at a 1-W average pump power level. Recently, we have observed spontaneous intersubband emission from a four-level system pumped by a CO_2 laser.

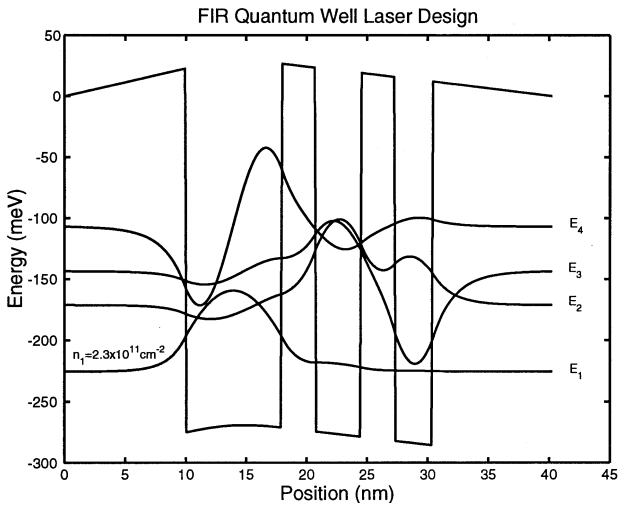

Figure 7. Schematic of a four-level system based on a coupled triple quantum-well structure. Electrons can be pumped from the E_1 to the E_4 level by a CO_2 laser. They then quickly relax to the E_3 level by LO-phonon scattering. Similarly, the electrons on the E_2 level can be emptied quickly to E_1 through LO-phonon scattering. THz emission takes place between E_3 and E_2.

3.3.3 Mid-infrared Quantum-cascade Lasers

Sponsor

U.S. Army Research Laboratory/Federated Laboratory
Grant QK-8819

Project Staff

Benjamin S. Williams, Brian P. Riely, Professor Qing Hu, in collaboration with Professor Michael R. Melloch[6]

High-power, compact mid-infrared (8-12 micron) lasers are very useful tools for remote sensing, endpoint detection in dry etching processes, point-to-point communication, and night vision applications. Conventional laser diodes operating in this long wavelength range use narrow-gap lead-salt semiconductors, which require cryogenic operations, provide relatively low power levels, and have very limited frequency tunability. Recently developed quantum-cascade (QC) lasers based on intersubband transitions have shown much higher operating temperatures and a great frequency tunability. These features make them ideal for the above-mentioned applications. In this project, we are developing mid-infrared quantum-cascade lasers based on GaAs/AlGaAs quantum-well structures. Compared to the InGaAs/InAlAs materials used in the original quantum-cascade lasers developed at Bell Labs, the GaAs/AlGaAs system offers a much higher thermal conductivity (approximately a factor of 20 compared to InGaAs/InAlAs) and therefore a higher-power operation.

The core of our MQW structure is a tightly coupled double quantum well, in which three energy levels form the three-level lasing structure. These energy levels are shown in Figure 8. The lasing transition is to take place between E_3 and E_2, with the energy separation approximately 120 meV, corresponding to 10-micron wavelength. The energy separation between E_2 and E_1 is designed to be approximately 36 meV, which is the energy of LO phonon in GaAs. Consequently, the energy level E_2 will be depopulated by very fast LO-phonon scattering (~0.2 ps). Our design of the MQW structures is aided by a numerical code that solves Shrödinger and Poisson equations self-consistently; and it includes the effect of band nonparabolicity to account for the much higher energy levels corresponding to infrared frequencies.

The superlattice structure sandwiching the active region serves the purpose of selective injection of electrons into the E_3 level, and selective removal of electrons from both E_2 and E_1 levels. By choosing the period of the superlattice properly, the Bragg reflection results in minigaps (transport forbidden) and minibands (transport allowed), as shown in both Figure 8 and Figure 9. The combination of the selective injection into E_3 and the fast removal from E_2 will assure an inverted population between these two levels. We calculated the dipole moment for the $E_3 \rightarrow E_2$ transition to be approximately 23 Å, which yields a modal gain of 480 cm^{-1} for a doping concentration of $1.5 \times 10^{11}/cm^2$. Such a high level of gain is characteristic of the QC lasers in which the two subbands track each other in momentum, resulting in a large joint density of states.

6 Purdue University, West Lafayette, Indiana.

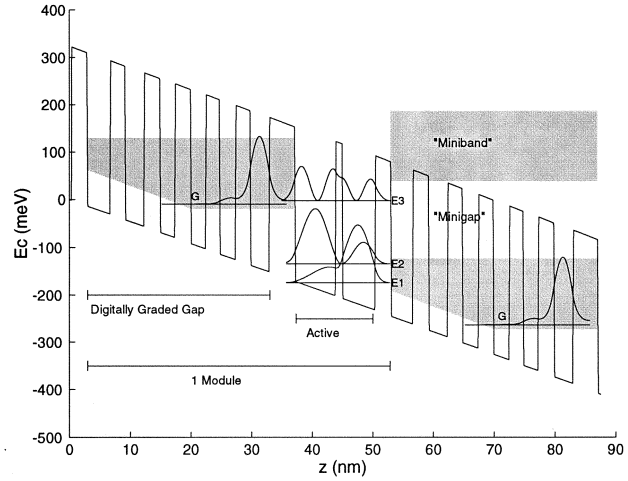

Figure 8. Conduction-band profile and wave functions of the designed MQW structure that contains a three-level gain medium and superlattices for selective injection and removal of electrons.

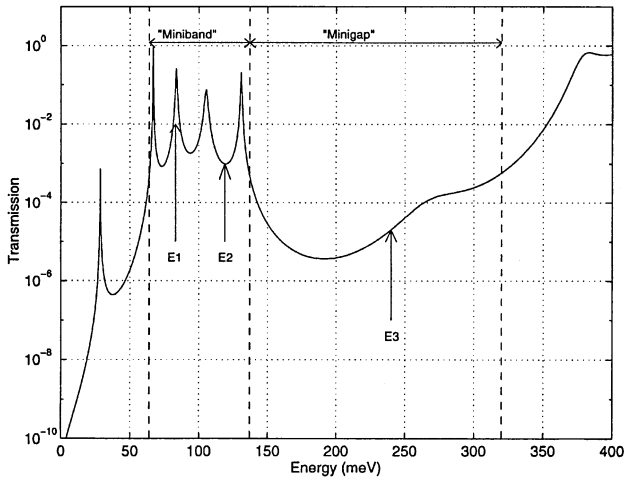

Figure 9. Calculated transmission coefficient of the superlattice sandwiching the core structure. The valley in the transmission corresponds to the minigap and the peaks form the miniband.

We have fabricated a MQW structure consisting of 40 nominally identical structures as shown in Figure 8. We have performed emission measurements using the FTIR system shown in Figure 5. An emission spectrum with the narrowest linewidth is shown in Figure 10. We designed for a center frequency of 121 meV, which corresponds to a 10-micron wavelength, and the FWHM linewidth is only 10.8 meV. This linewidth, comparable to the narrowest achieved at Bell Labs using InGaAs/InAlAs structures, is an indication of the high interface quality and uniformity of our MQW structures. Currently, we are designing suitable cladding layers for mode confinement to achieve lasing.

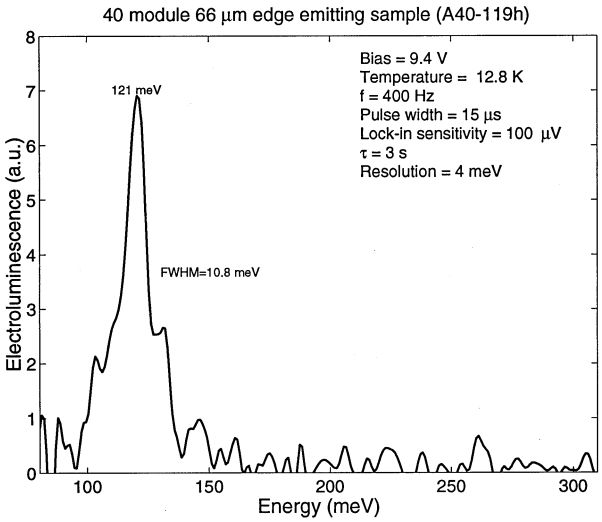

Figure 10. Spectrum of spontaneous intersubband emission from a 40-module MQW structure whose design is shown in Figure 8.

3.3.4 Picosecond Time-Resolved Transport Studies of Quantum-Effect Devices

Sponsor

National Science Foundation/MRSEC
Grant DMR 94-00344

Project Staff

Noah D. Zamdmer, Professor Qing Hu

Our previous work in frequency domain has yielded new information about quantum-effect devices. In a complementary approach, we are studying the response of the quantum devices in time-resolved fashion by using a pump-and-probe method with a pulsed laser. A 100-fs laser pulse contains frequency components up to 10 THz, which should enable us to perform spectroscopic studies on quantum devices over a broad frequency range that covers all the interesting energy levels, namely the intersubband transition and Coulomb interaction energies. Furthermore, and perhaps the most attractive feature of the time-domain studies, the time-resolved studies can reveal information that frequency-domain studies cannot reveal, namely the time scale of transport process in quantum devices. This is one of the basic issues in determining potential applications of the quantum devices.

In order to pursue the time-resolved pump-and-probe measurements on quantum-effect devices, we have constructed a cryostat with optical-fiber couplers that can bring sub-picosecond laser pulses to the cryogenic stage. The schematic of the system is shown in Figure 11, along with the schematic of coplanar transmission lines that provide the dc biases of the pump and probe Austin switches and the propagation path for the generated picosecond electrical pulses.

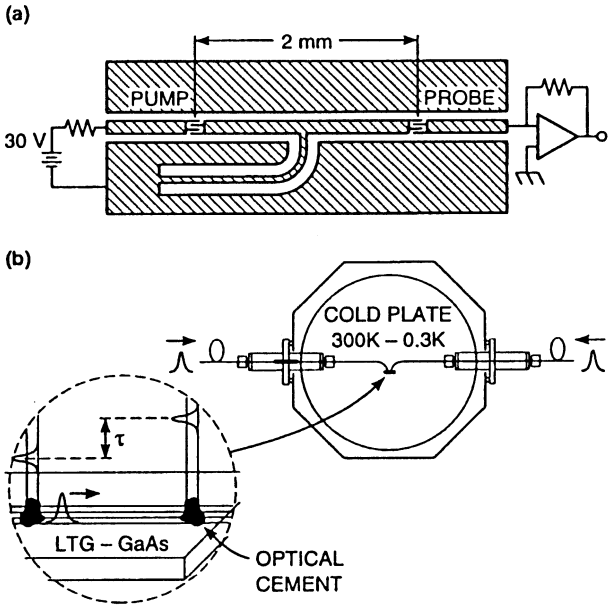

Figure 11. (a) Two Austin switches coupled through a coplanar transmission line. (b) Schematic of a cryostat with optical-fiber couplers that bring subpicosecond laser pulses to the cryogenic stage.

Our initial successful testing of the cryogenic pump-and-probe system was performed using the coupling structure shown in Figure 11. In this structure, two Austin switches are coupled through a coplanar transmission line without disruptions. This is the simplest coupling scheme to implement, and it provides an efficient propagation of the picosecond pulses with minimal attenuation and distortion. However, such a simple structure does not allow for easy insertion of a three-terminal device in between the pump and probe switches. To insert a three-terminal device, the ground planes surrounding the center conductor must be broken to allow two electrical contacts to the center conductor, which will be the source (on the side of the pump switch) and drain (on the side of the probe switch). Such broken ground planes will cause significant distortion and attenuation of the propagating pulses, making the measurement results difficult to interpret.

To overcome this difficult technical problem, we have developed a novel coplanar waveguide circuit whose schematic is shown in Figure 12. In this structure, the two isolated ground planes in the center can serve as two separate gate electrodes. The ground plane on the left can serve as the contact to the source, and the ground plane on the right can serve as the contact to the drain. Furthermore, each Austin switch has two separate dc biases. This way, if the optical illumination to the pump and probe switches is misaligned, unavoidable in a fiber-coupled cryogenic environment, the generated photocurrent can be compensated by the two biases, and a pure TEM mode can be generated and detected. Our preliminary measurements on this structure yielded encouraging results, showing the separate dc biases can largely compensate misaligned optical pulses.

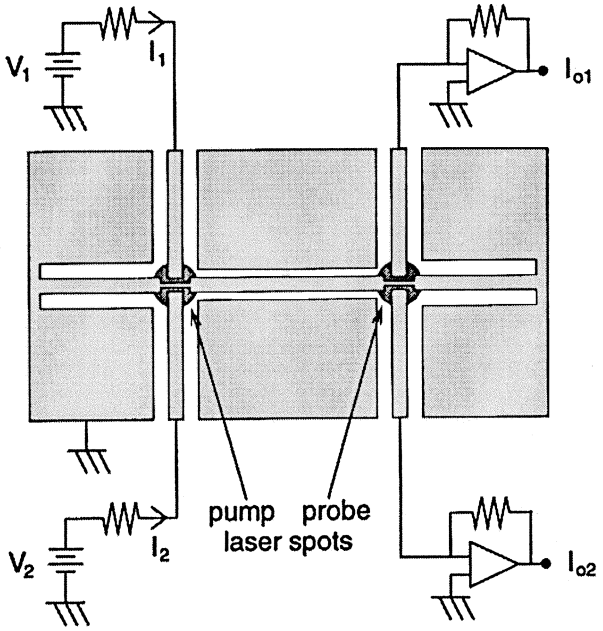

Figure 12. A novel coplanar waveguide structure that provides an easy integration with a three-terminal device and a compensation of misaligned optical pulses.

3.4 Publications

3.4.1 Journal Articles

del Alamo, J.A., C.C. Eugster, Q. Hu, M.R. Melloch, and M.J. Rooks. “Electron Waveguide Devices.” *Superlatt. and Microstruct.* 23: 121 (1998).

Lyubomirsky, I., and Q. Hu. “Energy Level Schemes for Far-infrared Quantum Well Lasers.” *Appl. Phys. Lett.* 73: 300 (1998).

Lyubomirsky, I., Q. Hu, and M.R. Melloch. “Measurement of Far-infrared Intersubband Spontaneous Emission from Optically Pumped Quantum Wells.” *Appl. Phys. Lett.* 73: 3043 (1998).

Zamdmer, N.D., Q. Hu, S. Verghese, and A. Förster. “Mode-discriminating Photoconductor and Coplanar Waveguide Circuit for Picosecond Sampling.” *Appl. Phys. Lett.* Forthcoming.

3.4.2 Book Chapters

Hu, Q., B. Xu, and M.R. Melloch. “Intersubband Terahertz Emitters.” In *Future Trend in Microelectronics*, S. Luryi, J. Xu, A. Zaslavsky, eds. New York: John Wiley. Forthcoming.

Xu, B., Q. Hu, and M.R. Melloch. “Intersubband THz Emission in Multiple Quantum Wells.” In chapter 10, “Long Wavelength Infrared Emitters Based on Quantum Wells.” Volume 9 in *Optoelectronic Properties of Semiconductors and Superlattices.* M. Helm, ed. New York: Gordon and Breach. Forthcoming.

3.4.3 Meeting Papers

de Lange, K. Konistis, Q. Hu, R. Robertazzi, and D. Osterman. “A Low-noise, 9-element Micromachined SIS Imaging Array.” Paper presented at the 9th International Symposium on Space Terahertz Technology, Pasadena, California, March 1998. To be published in the symposium proceedings.

Hu, Q. “Terahertz Emitters Based on Intersubband Transitions.” Invited paper presented at the IEEE Lasers and Electro-Optical Society (LEOS), Meeting session WB3, Orlando, Florida, December 1998.

Williams, B., B. Riely, Q. Hu, and M.R. Melloch. “Mid-Infrared Quantum Cascade Lasers.” Paper presented at the 1998 APS March meeting in session Q27.02, Los Angeles, California, March 1998.

Xu, B. “Electrically Pumped Terahertz Emitter based on Intersubband Transition.” Invited paper presented at the 1998 American Physical Society March meeting, session U21.01, Los Angeles, California, March 1998.

3.4.4 Theses

Konistis, K. *Development of a 3×3 Micromachined 190 GHz SIS Imaging Array*. S.M. thesis. Department of Electrical Engineering and Computer Science, MIT, May 1998.

Williams, B. *GaAs/AlGaAs Mid-infrared Quantum Cascade Laser.* S.M. thesis. Department of Electrical Engineering and Computer Science, MIT, May 1998.

3.4.5 Doctoral Dissertations

Lyubomirsky, I. *Toward Far-infrared Quantum Well Lasers*. Ph.D. diss. Department of Electrical Engineering and Computer Science, MIT, November 1998.

Xu, B. *Development of Intersubband Terahertz Lasers Using Multiple Quantum Well Structures*. Ph.D. diss. Department of Electrical Engineering and Computer Science, MIT, August 1998.

;